2494–2502 *Nucleic Acids Research, 1999, Vol. 27, No. 12*

Analysis of the cooperative thermal unfolding of the *td* intron of bacteriophage T4

Philippe Brion[1,2], François Michel[2], Renée Schroeder[3] and Eric Westhof[1,*]

[1]Institut de Biologie Moléculaire et Cellulaire du CNRS, UPR 9002, F-67084 Strasbourg, France, [2]Centre de Génétique Moléculaire du CNRS, F-91190 Gif-sur-Yvette, France and [3]Institute of Microbiology and Genetics, Vienna Biocenter, Dr Bohrgasse 9, A-1030 Vienna, Austria

Received March 3, 1999; Revised and Accepted May 3, 1999

ABSTRACT

The thermal stability of folded transcripts of the *td* intron of bacteriophage T4 that carried up to three base substitutions was investigated by temperature gradient gel electrophoresis (TGGE) and UV melting. The unfolding of this autocatalytic group I intron is endothermic and entropically driven. Although the effects of mutations in base pairs follow in most cases the expected order G-C>A-U>G·U>A·C, the extent of global destabilization varies strongly according to the helix in which substitutions are located. Effects are more pronounced in the P7 helix which forms, together with the P3 helix, the central pseudoknot of group I introns. The stability of the tertiary fold was also monitored as a function of ionic concentration and of the nature of the ion. At low ionic strength, the stabilizing effect of divalent ions is independent of the nature of the ion. However, with increasing ionic concentration, stabilization is most pronounced for Mg^{2+} and less for Mn^{2+} with Ca^{2+} having intermediate effects. Ammonium ions stabilize folding with a similar slope, but at concentrations about 400 times higher than divalent ions. The apparent enthalpic change associated with the tertiary structure thermal unfolding increases strongly with increasing concentrations of divalent ions. A similar increase is observed with the monovalent ammonium ions. However, in the presence of NH_4^+ ions, the apparent enthalpy peaks at 2.0 M and decreases beyond.

INTRODUCTION

Despite a uniformly charged backbone, complex catalytic RNAs, such as group I introns, possess a well-defined, stable tertiary structure in the presence of magnesium ions (1–3). The three-dimensional architecture of group I intron molecules is composed of two main structural domains, P4-P5-P6 and P3-P7-P8, that form, by proper association, the active site of the ribozyme (4–6). Further details about the architecture of group I introns have now become available with the recent publication of a medium-resolution crystallographic structure of the entire core of the *Tetrahymena* intron (7).

While large-scale studies of the thermodynamics of RNA secondary structure formation in model compounds are available (8), much remains to be learnt about the thermodynamic aspects of tertiary structure formation in large RNA molecules. Within a hierarchical approach to RNA folding (9), the helices belonging to secondary structure (defined as composed of contiguous Watson–Crick base pairs) form first. Then, in a second step, remaining unpaired sections (single-stranded and loop segments) organize the tertiary contacts allowing the self-assembly of RNA three-dimensional architecture. The simplest demonstration of a well-defined, stable tertiary structure is provided by UV melting curves, as already shown for tRNAs (10,11), a fragment of ribosomal RNA (12,13), several group I introns (14–16) and a group II intron (17,18). In the cases investigated (reviewed in 19,20), melting experiments usually revealed two well separated transitions; the first one—occurring within a small temperature range and therefore considered as very cooperative—was attributed to the melting of tertiary structure, while the other, generally broader one was regarded as reflecting the disruption of secondary structures at higher temperatures. For group I and group II introns, the temperature of the first transition coincides with the temperature of inactivation and direct evidence as to the physical origin of observed transitions was obtained by chemical modification and activity measurements (14,15,18). A majority of the residues affected in their accessibility to chemical modification during the major initial transition were found to be in single-stranded segments, as would be expected for the unfolding of most if not all of the tertiary structure. However, part of the P3 and P7 helices, which constitute the central pseudoknot of group I introns, are found to melt before the rest of the secondary structure, concomitantly with the loss of tertiary interactions (15). Indeed, the P3-P7 pseudoknot, because it involves distant segments of the molecule, is unlikely to form before much of the secondary structure has already come into existence. Zarrinkar and Williamson confirmed that, *in vitro*, P4 and P6 are formed earlier than P3 and P7, the formation of which coincides with the rate-limiting step for activity (21).

Previous work on group I introns showed that their overall thermal stability could be altered by changing a single or a few nucleotides involved in long range tertiary interactions (15,22). In this study, we develop further this approach by quantitatively investigating the destabilizing influence of specific base-pair substitutions, located in helices, on the thermal stability of the *td* group I intron. Our approach is purely thermodynamic and

*To whom correspondence should be addressed. Tel: +33 3 88 41 70 46; Fax: +33 3 88 60 22 18; Email: westhof@ibmc.u-strasbg.fr

the questions we ask pertain to the role of given helices and divalent and monovalent ions in the stability of the global tertiary structure. With the aim of investigating the relationship between the extent of destabilization caused by a base substitution in a helix and its location, mutations were introduced in the P9 and P6a pairings, as well as in the two helices, P3 and P7, that constitute the central group I pseudoknot (Fig. 1). Since divalent ions are necessary for RNA folding, the contributions of three divalent cations, Mg^{2+}, Ca^{2+} and Mn^{2+}, to the stability of the *td* group I intron were also investigated and compared to the stabilizing effects of the monovalent ammonium ions. Further, because a conformationally homogeneous RNA population is a prerequisite for quantitative interpretation of UV-melting experiments, different nucleotide sequence variants of the *td* intron were also analyzed by temperature gradient gel electrophoresis (TGGE).

MATERIALS AND METHODS

DNA constructs

The *td*-derived ribozyme used in this work is described in (23). Nucleotide substitutions were introduced by standard mutagenesis procedures (24). All constructs were verified by sequencing the entire length of the insert.

In vitro transcription, RNA purification and renaturation

DNA templates were generated by PCR using the following primers: 5'-ATTTAATACGACTCACTATAGAATCTATC-TAAAC- 3' (T7 promoter underlined) defines the 5' extremity and 5'-TGTTCAGATAAGGTC-3' the 3' extremity. RNA synthesis was as described in (15), except that higher concentration ratios of magnesium ions over nucleotides were used during transcription by T7 RNA polymerase.

All transcripts were purified from acrylamide–urea gels. Elution was in 10 mM Tris–HCl (pH 7.5 at 25°C), 250 mM NaCl, 1mM Na_2EDTA. After passive elution, the volume of the filtered supernatant was precipitated in the presence of 3 M sodium acetate. Pellets were rinsed twice with 70% ethanol before drying and resuspended in water. RNA concentrations were estimated from absorbance at 260 nm.

Each particular RNA to be renatured was incubated at a temperature within its melting range for 10 min and then allowed to cool slowly to room temperature (25°C) after 5× concentrated buffer was added.

UV melting curve analyses

Samples were adjusted to an approximate absorbance of 0.250 in 50 mM NaCacodylate (pH 7.5), 50 mM NH_4Cl and the appropriate concentration of the ion studied. Samples were degassed under vacuum prior to collecting melting data. Absorbance was measured at 260 nm with a heating rate of 0.2°C/min on a Uvikon 941 plus spectrophotometer (Kontron Instruments) equipped with two cells thermostated by a Neslab RTE 100 circulating bath coupled to a thermoprogrammer (Neslab Instruments). Data were collected from 30 to 80°C at 0.05°C intervals. Derivatives of absorbance versus temperature were generated using the locally weighted least squared error method provided by the Kaleidagraph program (Abelbeck Software) on a Macintosh computer. The thermodynamic parameters were derived as described in (25) assuming a simple model. Our model assumes that each transition—tertiary structure unfolding on one hand and secondary structure unfolding on the other—is a continuous process over a given temperature range during which a folded population unfolds. We therefore deconvoluted the derivative curve assuming that each transition follows a gaussian distribution G(T; S, σ, Tm). In the dA/dT versus T representation, each transition is parametered by S, a correction factor for the surface of the gaussian; σ, the standard-deviation and Tm, the temperature where the function reaches a maximum, a good approximation for the melting temperature. The theoretical profile is then written as the sum of the constitutive transitions:

$$P_{calc} = \sum_i G_i\,(T; S_i\, \sigma_i, Tm_i)$$

To estimate the S_i, σ_I and Tm_i, the difference between the experimental and theoretical profiles was minimized by a least squared error method in the Excel program.

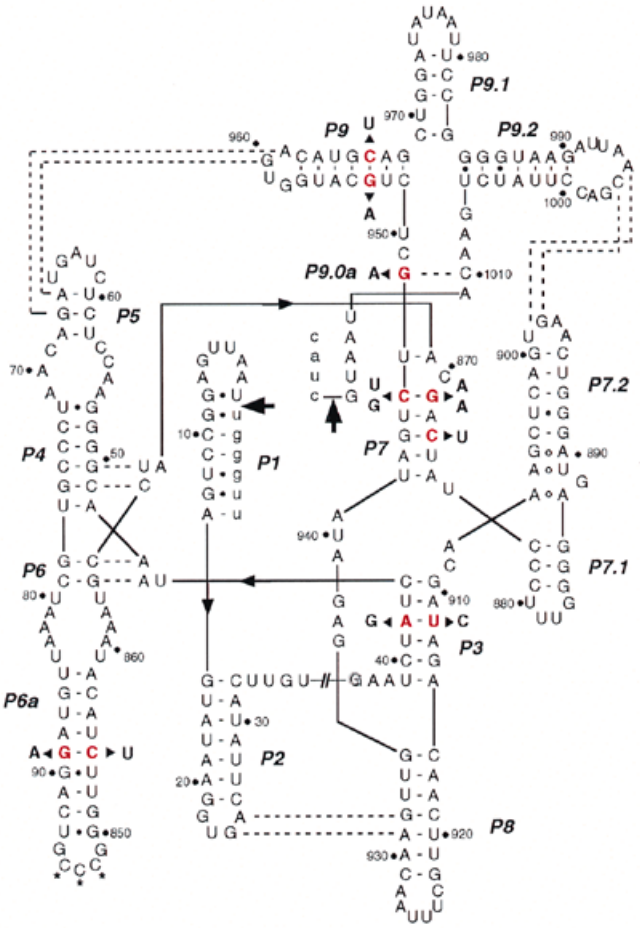

Figure 1. Secondary structure model of the *td* group I intron of bacteriophage T4 (49), redrawn after (50). Heavy arrows point to splice junctions, exons are in lower case. Tertiary interactions are indicated by broken lines. Numbering of the intron sequence is according to (51). Nucleotides substituted in this study are in red boldface letters. The truncated ribozyme form of the intron used for melting experiments begins with a surnumerous G (shaded) after the // symbol (23). Asterisks indicate the position of the open reading frame that was deleted in the constructs used in this work (52). The junction between P7.1 and P7.2 follows the proposal of (53).

Calculated Tm values are based on nearest neighbor thermodynamic parameters (8,26,27).

Temperature-gradient gel electrophoresis

TGGE experiments were performed essentially as previously described (28). The instrument used was the commercially available TGGE system (DIAGEN). Native polyacrylamide gels (5%) containing 20 mM MOPS (pH 7.5) and 5 mM magnesium acetate were set between one glass plate and a GelBond film (FMC BioProducts). The hydrophobic side of the GelBond film was in contact with the glass plate, the hydrophilic side being covalently linked to the gel to avoid deformation at high temperature. Gels were 1 mm thick. RNA samples were renatured as described above. After renaturation, wild-type and mutant transcripts were mixed if necessary and glycerol was added to 10% final concentration. The gel was loaded with 100–300 µl samples. It was then electrophoresed at room temperature and low voltage to ensure entry of the sample into the gel matrix. After 30–45 min of electrophoresis, the gel was placed onto the pre-equilibrated aluminium plate and covered with glass plates for thermal insulation. The temperature gradient was established perpendicular to the electric field using two thermostated baths. In reference runs the linearity of the temperature gradient used was tested inside the gel by thermoresistors. The deviation from linearity was checked several times to be <1°C everywhere in the gel. RNA was allowed to equilibrate for 10 min and was then electrophoresed at 500 V for 1.5 h. The gels were visualized by silver staining (29). To determine the transition temperature, the position of the midpoint of the transition was estimated and the temperature obtained from the reference linear gradient. Repeat experiments yielded transition temperatures within ±1°C of one another.

RESULTS

Monitoring of the conformational transitions of *td* ribozyme transcripts by TGGE

TGGE (28) of a sample of RNA molecules makes it possible to detect the presence of multiple conformers and to estimate the thermal stability of each of them in a single experiment. A continuous temperature gradient is applied perpendicular to the direction of migration in a non-denaturing gel, so that temperature-induced structural transitions can be visualized as spatially localized changes in electrophoretic mobility.

In Figure 2A, the TGGE profile of the wild-type *td* intron transcript is shown from 40 to 70°C. Under these conditions, wild-type *td* intron molecules run as a single band at low temperature, indicating the presence of only one major conformer. At higher temperatures the RNA undergoes a monophasic transition, seen as a shift in mobility, with a Tm value ~56°C. This value coincides with the Tm of the first peak in absorbance melting profiles of the wild-type *td* molecule (see below and Fig. 3) and, accordingly, we interpret this transition as reflecting the cooperative melting of the three-dimensional structure of the *td* intron. Because the observed transition is continuous, the process it visualizes must be reversible under the conditions of electrophoresis (30). As expected from the presence of magnesium ions, a smear caused by RNA degradation becomes visible around 60°C.

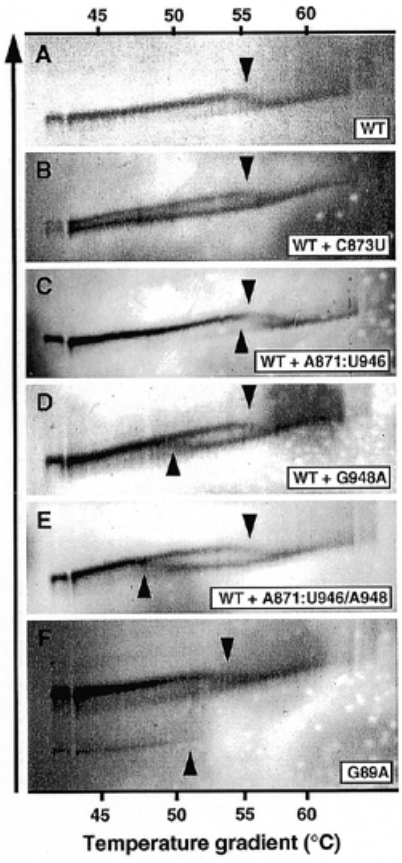

Figure 2. Perpendicular TGGE-melting profiles of various *td* group I intron transcripts. (**A**) Wild-type *td* group I intron transcript. (**B**) Wild-type and single substituted C873U mutant. (**C**) Wild-type and double-substituted A871:U946 mutant. (**D**) Wild-type and single substituted G948A mutant. (**E**) Wild-type and triple-substituted A871:U946 and G948A mutant. (**F**) Single substituted G89A mutant. For this mutant, in addition to the main band and the band correponding to the dimer, another band of low intensity can be observed because of longer developing time and the use of twice as much RNA as for other mutants. Electrophoresis was performed in 20 mM MOPS–KOH (pH 7.5 at 25°C), 5 mM $Mg(OAc)_2$ as described in Materials and Methods. The arrow heads point to the melting transitions. The arrow indicates the sense of migration.

In the TGGE profile of a mixture of wild-type and, in the helix P7, singly substituted C873U mutant molecules (Fig. 2B), two bands can already be distinguished at the lowest temperature of the gradient, which shows that the two transcripts have distinct conformations. Since the slower migrating band merges with the other one at the temperature expected for the main monophasic transition of the wild-type RNA (compare Fig. 2B with A), it can be concluded that the molecules in that band already lack most if not all of the wild-type tertiary structure at low temperatures. In contrast, another substitution in helix P7 (G871A-C946U) results in a wild-type-like migration except that the transition is shifted towards lower temperatures with a Tm value close to 53°C (Fig. 2C). The assignment of a band to mutant molecules was confirmed by running the same transcript separately on another gel (data not shown).

In Figure 2D, the TGGE profile of a mixture of wild-type molecules with transcripts carrying a single substitution (G948A) in helix P9.0a is shown. A clear difference in the

higher-order stability of the two RNA species is apparent in this temperature range, since the Tm of the mutant transcript (49°C) is ~7°C lower than that of the wild-type. Interestingly, a diffuse slower migrating band is observed at low temperatures, suggesting the presence of more than one conformer. Conformational inhomogeneity has similarly been invoked to account for the incomplete reactivity of molecular populations of the closely related *sunY* intron (15,31) and was also observed on native gels by Emerick and Woodson for the *Tetrahymena* intron (32).

Figure 2E shows the TGGE profile of a mixture of triple-substituted G948A/G871A-C946U mutant transcripts, disrupting P7 and P9.0a simultaneously, and wild-type molecules. As in Figure 2C, the significantly different shapes of the wild-type and G948A/G871A-C946U bands result from the lower thermal stability of the mutant molecules, which have a Tm of ~47°C. Interestingly, comparison of Figure 2C, D and E suggests that at the resolution of the gel, the mutations A948 and A871-U946 have additive effects. The TGGE profile of the G89A mutant (Fig. 2F) also reveals a dominant band with a transition around 52°C. However, a minor, very slowly migrating band is also observed at lower temperatures. The molecules in this band, which disappears around 52°C, could result from the partial dimerization of the intron. Indeed, in TGGE experiments, the RNA molecules are allowed to assume their equilibrium conformations at each temperature of the gradient before application of the electric field and, thus, a discontinuous transition points to strand separation (30). More specifically, we suggest that dimerization results from the partial destabilization of the P6a element and involves the L6a loop. Formation of a helix between two intron molecules would implicate the imperfect palindrome GCCCGGGU. By using the thermodynamical data provided by Serra and Turner (8), we calculate for this intermolecular helix a Tm of 55°C and this value agrees well with our experimental data (assuming a concentration similar to that used in UV melting experiments, see below).

To summarize, bands tend to be fairly homogeneous in most of our TGGE profiles (<10% of the material in smears) until ~55°C. In most cases, a single band is observed at low temperatures, just as expected for a population of molecules dominated by a single conformer, a situation ideal for conducting UV melting experiments.

Probing individual interactions by UV absorbance versus temperature curves

Monitoring of UV absorbance as a function of temperature has been used to follow the overall unfolding of several group I introns under a variety of conditions (14–16,33). When *td* wild-type transcripts are heated in a buffer containing 5 mM $MgCl_2$, an initial unfolding transition is observed to give rise to a major peak in the first-derivative absorbance versus temperature profile (Fig. 3). The width of the transition suggests a highly cooperative process. Similar early occurring and highly cooperative transitions were observed for the *Tetrahymena* (14) and *sunY* (15) group I introns and shown in both cases to reflect the disruption of the three-dimensional structure of the molecule.

In order to assess the contribution of various helical elements to the global stability of the *td* intron, we chose to introduce substitutions in the P7, P3, P9.0a, P9 and P6a pairings. The first two pairings correspond to the two constitutive helices of the central group I pseudoknot, whereas the last two may be considered as classical secondary structure pairings. The mutant G948A in P9.0a, already characterized (15), was used as an internal reference. In all instances, destabilizing a single

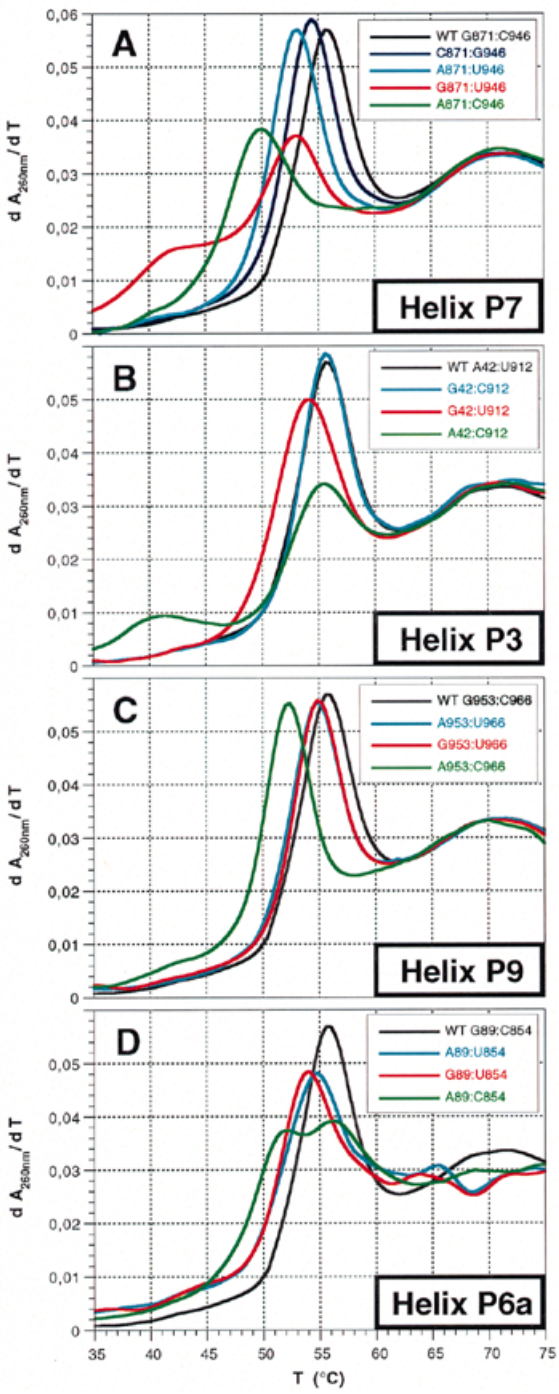

Figure 3. Melting curves for various *td* group I intron transcripts. The first derivative profiles (dA/dT) are shown. (**A**) Melting profiles of the wild-type and various mutants affecting the P7 pairing. (**B**) Melting profiles of the wild-type and various mutants affecting the P3 pairing. (**C**) Melting profiles of the wild-type and various mutants affecting the P9 pairing. (**D**) Melting profiles of the wild-type and various mutants affecting the P6a pairing. Derivative absorbance melting profiles were determined in 50 mM NaCacodylate (pH 7.5 at 25°C), 50 mM NH_4Cl and 5 mM $MgCl_2$.

Table 1. Thermodynamic parameters calculated from absorbance versus temperature profiles[a]

Element	Mutation	Tm ± 0.2 (°C)	ΔTm (°C)	$-\Delta H^0$ (kcal/mol^{-1})	$-\Delta S^0$ (e.u.)	ΔG^0_{37} (kcal/mol^{-1})	$\Delta\Delta G^0_{37}$[b] (kcal/mol^{-1})
P7	G871-C946 (wt)	55.2	/	154	469	–8.5	/
	C871-G946	53.9	1.3	152	465	–7.8	0.7
	A871-U946	52.6	2.6	146	448	–7.0	1.5
	G871-U946	54.6	0.6	126	384	–6.9	1.6
	A871-C946	49.5	5.7	103	319	–4.1	4.4
P3	A42-U912 (wt)	55.2	/	154	469	–8.5	/
	G42-C912	55.1	0.1	164	499	–9.2	–0.7
	G42-U912	53.5	1.7	126	385	–6.6	1.9
	A42-C912	54.3	0.9	121	369	–6.6	1.9
P9	G953-C966 (wt)	55.2	/	154	469	–8.5	/
	A953-U966	54.3	0.9	158	482	–8.5	0.0
	G953-U966	54.4	0.8	169	516	–8.9	–0.4
	A953-C966	51.8	3.4	173	532	–8.0	0.5
P6a	G89-C854 (wt)	55.2	/	154	469	–8.5	/
	A89-U854	54.0	1.2	154	470	–8.2	0.3
	G89-U854	53.4	1.8	165	505	–8.4	0.1
	A89-C854	50.6	4.6	169	522	–6.6	1.9

[a]See Materials and Methods.
[b]$\Delta\Delta G^0_{37} = \Delta G^0_{37}$(mutant) – ΔG^0_{37}(wild-type).

Watson–Crick pair results in shifting the first melting transition to lower temperatures and starting with a G-C pair, relative extents of destabilization are typically as expected, with molecules carrying an A-U usually being less destabilized than those with a G•U pair, which tend in turn to be more stable than A•C mutants (Fig. 3). However, the effects of a given type of substitution are strongly dependent on the helix in which it is located. For instance, while mutations affecting the P7 pair (which binds the guanosine cofactor of group I splicing) are already among the most destabilizing ones (Fig. 2), the C873U mutant in the middle of the same helix is even more severely affected, to the point that there is no discernable peak corresponding to the melting of the three-dimensional structure. Interestingly, even replacing the G-C base pair that forms the G-binding site in P7 by a C-G pair is slightly destabilizing. In comparison with P7, mutations in the other helix of the core pseudoknot, P3, have less severe effects and their melting profiles are more comparable to those of mutations in P9 and P6a. Three mutants exhibit a complex melting profile. The U912C mutant in P3 and the C946U mutant in P7 show an additional early transition around 42°C, suggesting the presence of another RNA population with a less stable fold. A third mutant, A89-C854 in P6a, exhibits a twin-peaked transition with Tm values of 51.4 and 55.6°C; we checked that varying the RNA concentration does not change the relative amplitudes of the two peaks and concluded that none of them can be attributed to the postulated dimer. Finally, we showed that some mutations have additive effects (Fig. 4): combining an A-U pair at the G-binding site with an A•C one in P9.0a shifts the major peak by roughly the same amount as the sum of the individual shifts, indicating that mutations at those two sites have effects on stability

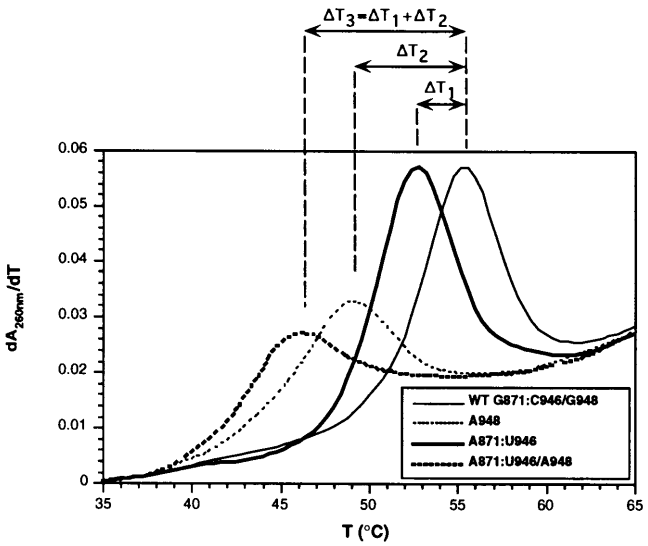

Figure 4. Additivity of the effects of mutations affecting long range interactions in the *td* group I intron core. ΔT_1 = Tm(wild-type) – Tm(A871U946), ΔT_2 = Tm(wild-type) – Tm(G948A) and ΔT_3 = Tm(wild-type) – Tm(A871U946/G948A).

independent from each other. The derived thermodynamic parameters are given in Table 1.

Effects of cations on the unfolding of tertiary structure

Magnesium ions are known to stabilize group I intron tertiary structure so that reducing or increasing their concentration results in shifting the early transition towards lower or higher

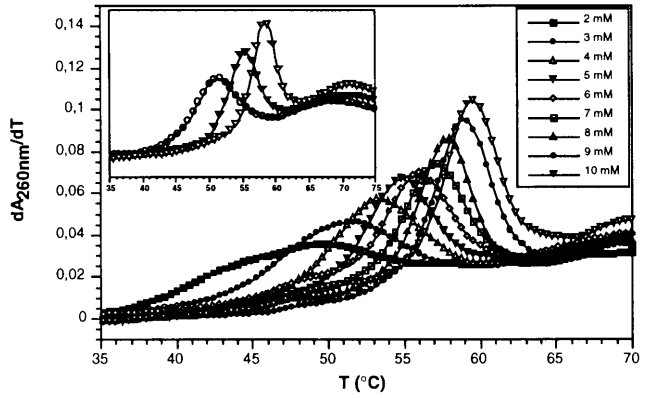

Figure 5. Stabilization of the wild-type *td* group I intron transcript by Mg^{2+} in the 2–10 mM range. Derivative absorbance melting profiles were determined in 50 mM NaCacodylate (pH 7.5 at 25°C), 50 mM NH_4Cl and various concentrations of $MgCl_2$.

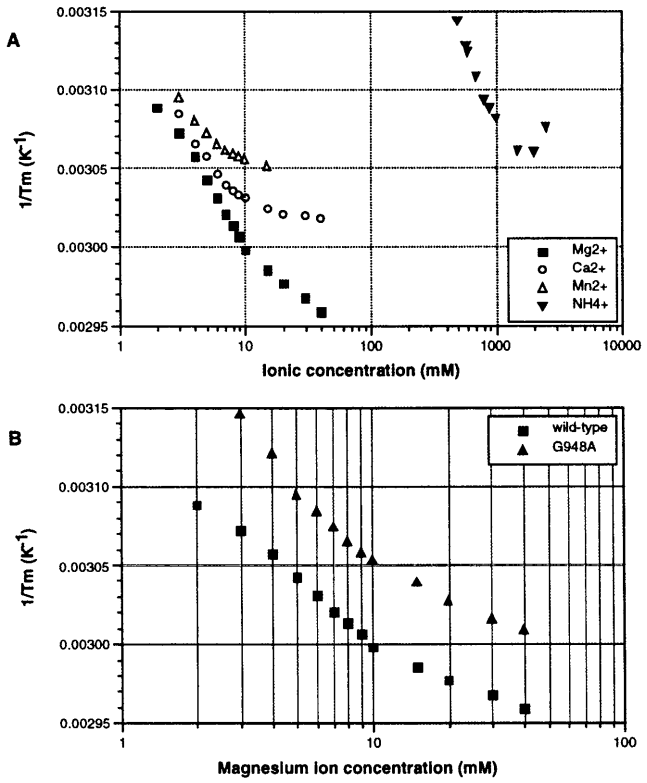

Figure 6. Dependence of Tm on divalent cation concentration. (**A**) 1/Tm as a function of ionic concentration for the three-dimensional melting transition of the wild-type *td* group I intron in the presence of the divalent Mg^{2+} (square), Ca^{2+} (circle), Mn^{2+} (open triangle) and monovalent NH_4^+ (closed downward triangle) cations. (**B**) 1/Tm as a function of log [Mg^{2+}] for the three-dimensional melting transitions of the wild-type *td* group I intron (square) and its mono-substituted G948A mutant (closed upward triangle). Melting experiments were conducted in 50 mM NaCacodylate (pH 7.5 at 25°C), 50 mM NH_4Cl.

temperatures, respectively (14,16). In order to quantitatively estimate these effects, *td* intron transcripts were submitted to UV melting experiments at different ionic concentrations. Figure 5 shows that when the concentration of magnesium was varied, the initial transition was shifted by approximately –5°C by going from 5 to 2 mM Mg^{2+} and by +5°C by going from 5 to 10mM Mg^{2+}. It may also be noted that the cooperativity of this transition decreases at low magnesium concentrations, in line with previous observations on other RNAs (10,14,17,19). However, a feature specific to the *td* group I intron melting profiles is that the first transition, corresponding to the melting of the three-dimensional structure, becomes distinct only at Mg^{2+} concentrations >2 mM. In contrast to the effects of Mg^{2+} on tertiary unfolding, the broad peak centered around 72°C (which corresponds to unfolding of secondary structure elements) remained essentially unaffected.

The dependence of the *td* intron melting temperature on Mg^{2+} concentration up to 40 mM is shown in Figure 6A. The curve exhibits an inflection point around 10 mM, the slope of the curve becoming less steep beyond this Mg^{2+} concentration. The dependence is, however, approximately linear over the 3–10 mM Mg^{2+} range. Figure 6A also shows the differential effects of Mg^{2+}, Ca^{2+} and Mn^{2+} on the stability of the *td* intron. It is clear that the divalent cations differ in their effectiveness at stabilizing the intron, with the order being Mg^{2+}>Ca^{2+}>Mn^{2+} (data for Mn^{2+} over 15 mM were judged unreliable due to significant RNA hydrolysis at high temperatures). At ion concentrations below 5 mM, the slopes of the three curves appear identical. However, their inflection points are different: 10 mM for Mg^{2+}, 7 mM for Ca^{2+} and 6 mM for Mn^{2+}. The difference in thermal stability between the wild-type and the G948A mutant observed at 5 mM Mg^{2+} concentration (Fig. 6B) is confirmed by the analysis of their melting profiles at other Mg^{2+} concentrations: upon addition of Mg^{2+}, both RNAs are stabilized to the same extent. The data suggest that divalent ions, especially Mg^{2+}, are binding specifically to sites present only in the folded state (34). A likely explanation for strong linear increase in the apparent enthalpy of the transition over the Mg^{2+} range considered (Fig. 7; Table 2) is that Mg^{2+} ions help organize the intron structure into a form with more negative enthalpy (11,12,34). The apparent enthalpy of lowest temperature transition is 127 kcal/mol with 5 mM Ca^{2+} in contrast to 150 kcal/mol at the same Mg^{2+} concentration, further suggesting that the *td* group I intron tertiary structure chelates Mg^{2+} ions in specific ways.

We wished to find conditions under which *td* intron transcripts fold into their tertiary structure in the absence of Mg^{2+} ions, so that interactions with Mg^{2+} ions could be studied independently of folding reactions. We therefore melted *td* intron transcripts in buffers with increasing concentrations of NH_4Cl. A new transition appears at ~45°C when 0.5 M NH_4Cl is reached. This transition, sharp and well resolved from the higher-temperature unfolding transition, was attributed to the tertiary structure unfolding. Because EDTA was included in the purification of the RNA, we exclude that contaminating divalent ions are responsible for folding in these experiments (Materials and Methods). So, while *td* intron transcripts appear to adopt a folded tertiary structure in the absence of divalent ions, a much greater molar concentration of NH_4^+ ions is required to observe the same extent of stabilization as can be obtained with Mg^{2+} ions. For instance, the same extent of stabilization obtained at 1.5 M NH_4^+ is achieved with a 375-fold lower concentration of Mg^{2+} ions. The enthalpy of the

Table 2. Melting temperatures and apparent enthalpies of transition calculated from absorbance versus temperature profiles as a function of ionic concentrations of three different ions

Ionic concentration (mM)	Mg^{2+}		Ca^{2+}		Mn^{2+}	
	Tm (°C)	ΔHapp (kcal/mol)	Tm (°C)	ΔHapp (kcal/mol)	Tm (°C)	ΔHapp (kcal/mol)
2	50.7	62				
3	52.4	89	51.1	89	49.9	99
4	53.9	118	53.1	110	51.5	105
5	55.6	150	53.9	127	52.4	138
6	56.7	176	55.1	162	53.1	128
7	58.0	181	55.9	147	53.5	140
8	58.7	215	56.3	142	53.8	151
9	59.5	198	56.5	171	54.0	145
10	60.4	216	56.8	158	54.2	162
15	61.8	217	57.5	180	54.6	171
20	62.7	261	57.9	209		
30	63.8	257	58.0	202		
40	64.8	274	58.2	222		

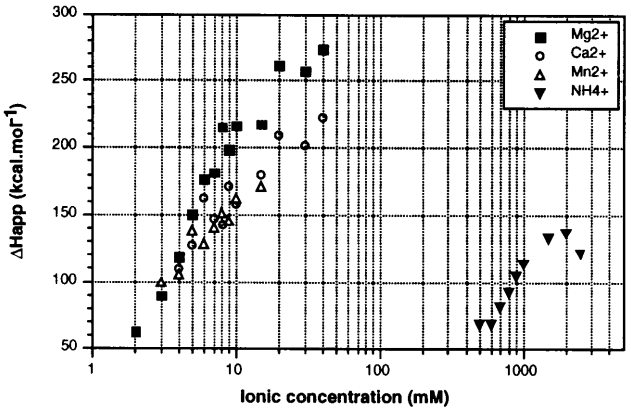

Figure 7. Dependence of the apparent ΔH on ionic concentration. Melting experiments were conducted in 50 mM NaCacodylate (pH 7.5 at 25°C), 50 mM NH_4Cl and various concentrations of additional ions: Mg^{2+} (square), Ca^{2+} (circle), Mn^{2+} (open triangle) and NH_4^+ (closed triangle).

Table 3. Melting temperatures and apparent enthalpies of transition calculated from absorbance versus temperature profiles as a function of ionic concentrations of ammonium ions

$[NH_4^+]$ (mM)	Tm (°C)	ΔHapp (kcal/mol)
500	45.1	68
600	47.1	68
700	49.0	81
800	50.4	92
900	50.6	104
1000	51.3	113
1500	53.6	132
2000	53.6	136
2500	51.4	121

transition shows about the same dependence on the log of ion concentration for monovalent and divalent ions (Fig. 7 and Table 3). However, with monovalent ions, the apparent enthalpy peaks at 2 M and then appears to decrease (no point could be obtained above 2.5 M due to RNA precipitation).

DISCUSSION

In this work, two different approaches have been applied to the study of thermal unfolding of the T4 *td* ribozyme—TGGE and the monitoring of UV absorbance. Because the information provided by UV absorbance is averaged over all structures present in solution it is important that the initial, undenatured sample be composed of homogeneously folded molecules in order to extract thermodynamic data from UV melting experiments. It was therefore necessary to complement UV melting with a method that allows us to check conformational homogeneity and also provides qualitative diagnostic information about the stability of the molecules under study. We thought of the TGGE method since it allows us to monitor gel mobility as a direct function of increasing temperature. The method was initially introduced to analyze the conformational transitions of double-stranded RNA (28). During the course of this work, TGGE was applied to the study of single-stranded RNA (35,36) and to studies of tertiary structure in tRNAs (37) and the P4-P6 domain of the *Tetrahymena* ribozyme (38). We have extended TGGE to the analysis of the melting behavior of sequence variants of the *td* group I intron that have the same size as the original molecule but differ from it by one to three bases. We find that the analysis of RNA transcripts by TGGE is a good complement to UV melting curves, especially since two different mutants (or even more) can be applied to one and

the same gel and thereby compared under exactly the same ionic conditions. Moreover, TGGE is easy to implement using a commercially available gel electrophoresis instrument, consumes little RNA (even when unlabeled RNA is used, only ~100 ng are necessary for one run) and there is much freedom in choosing the buffer conditions.

Assessing the energetic contribution of single nucleotides

The thermal unfolding behavior of RNA rapidly becomes a complex problem as the size of the RNA increases. In the particular case of group I introns, although the identity of secondary structure elements is now firmly established (reviewed in 39), it is not yet possible to estimate their exact contribution to the global structure. The same is true of the central pseudoknot, whose energetic contribution to the overall fold remains to be measured even though it is known to be essential for activity. We introduced base substitutions in two peripheral helices and in the two helices P3 and P7 which constitute the group I intron pseudoknot. The two peripheral helices we chose to mutate are present in a majority of group I introns, but differ in that P9 is involved in a tertiary contact by its terminal loop, whereas P6a is not.

It appears that mutations in P6a are affecting both the peak corresponding to the melting of the three-dimensional structure and the section of the melting profile that corresponds to secondary-structure pairings. The observation that disruption of the P6a helix influences the temperature of the initial unfolding transition may be due to the fact that even a single-base substitution within a helix can bring the melting temperature of the helix near the temperature range over which tertiary structure is lost. Comparing the effects we observed with the ones estimated using Turner's thermodynamic data suggests that this is indeed the case. Replacing the G89:C854 base pair in P6a by an A:U or G·U base pair is calculated to decrease the Tm of the helix by 6.3 and 12.1°C, respectively, which could altogether explain the shoulder visible on the initial transition and modification of the secondary structure massif. On the contrary, predicted Tm values for the P9 helix variants stay strictly above 71°C, which is far above the Tm of the three-dimensional fold. Therefore, the destabilizing effects of the G953A mutation in the P9 helix are best attributed to an indirect effect on the geometry of the the L9:P5 contact, which is important for stabilization of the tertiary structure (22).

Helices P3 and P7 have in common that their individual strands are located relatively far from one another on the sequence of the intron and that they cannot be simultaneously included in a planar tree-like representation of the group I intron secondary structure, i.e. they form a tertiary motif called a pseudoknot. Formally, of the two helices constituting a pseudoknot, one of them should be considered as belonging to secondary structure and the other one to tertiary structure. However, there is no a priori rule to tell which one is which. Our results suggest that P3 and P7 are not equivalent from a thermodynamic point of view. Analysis of Table 1 reveals that all but one of the mutations in the P3 helix result in Tm shifts that are actually lower than the ones observed for classical secondary structure helices. In contrast, mutations in P7 bp2 appear to be the most destabilizing ones. For example, the ΔTm (–5.6°C) that results from an A·C mismatch is similar to the one caused by introducing the same mismatch in the isolated P9.0a Watson–Crick base-pair (ΔTm = –6.5°C). Since the latter interaction is regarded as a typical tertiary long-range one, it is the P7 helix, rather than the P3 helix, that is best viewed as resulting from tertiary interactions.

Morerover, different positions within the P7 helix are not equivalent. In the case of the guanosine-binding site (G871-C946), base substitutions appear to have moderate global structural effects, since all mutants investigated exhibit a distinct peak attributable to the melting of the tertiary structure. In the case of the *Tetrahymena* group I intron, direct structural studies using Fe(II)-EDTA failed to reveal any difference between the wild-type and mutant ribozymes (40). In contrast, the C873U mutant RNA generates no discernable absorbance change that would correspond to the melting of tertiary structure (data not shown). This mutant can therefore be assumed to have no structured three-dimensional folding, or else to have difficulty in forming a conformationally homogeneous population. However, under the resolution of the TGGE method, the mutant molecules migrate as a single band under conditions that ensure native folding of wild-type molecules, and that band remains parallel to the dyes, so that it seems reasonable indeed to assume that this mutant has lost the ability to adopt a native three-dimensional fold.

The U912C mutation in P3 and C946U mutation in P7 do not result in a significant ΔTm as far as tertiary structure is concerned, but the presence of additional peaks centered around 41 and 46°C, respectively, may indicate that only a fraction of molecules carrying these mutations fold correctly. In light of what is currently known of group I intron folding, it is tempting to propose that these mutations somehow impair the formation of the kinetic folding unit constituted by the P3 and P7 helices (formation of P7-P3 is a determining step in the acquisition of the native fold; 21,41,42). These single mutations, independently of their effect on the stability of the native structure, probably alter the pattern of folding in such a way that some molecules become trapped in alternative conformations (43,44).

Differential effects of divalent cations on tertiary structure stability

Although the importance of divalent ions, and particularly Mg^{2+}, for group I intron structure and function is widely recognized (45), there have been relatively few thermodynamic studies of their overall contribution to group I intron stability (14,16,33). The *td* group I intron is suitable for such investigations because its tertiary unfolding transition is well resolved from the higher-temperature (secondary structure) broad unfolding transition.

As observed for other group I introns, the first transition, corresponding to the melting of the tertiary structure, is dependent on divalent cations. In the case of the *td* intron, we found that when the Mg^{2+} concentration drops below 2 mM this transition is no longer seen. For the closely related *sunY* intron, Michel and coworkers observed complete precursor transcripts to become active between 2 and 3 mM Mg^{2+} (31). In light of the present work, it is reasonable to suppose that in that study no catalytically active tertiary structure was present under 2 mM Mg^{2+}.

When comparing divalent ions with one another, we found that, with increasing ion concentration, stabilization is most pronounced with Mg^{2+} and least with Mn^{2+}, with Ca^{2+} being intermediate. On the basis of metal ion supplementation

experiments conducted on the L-21 *Sca*I ribozyme (46) and the catalytic RNA subunit of RNase P (47) two distinct classes of metal binding sites were postulated: structural sites and those more directly involved in catalysis. These authors showed that Ca^{2+} can reduce Mg^{2+} and Mn^{2+} requirements for occupation of structural sites, while these latter ions are the only ones efficient for catalysis by these ribozymes. UV cross-linking experiments further support the conclusion that Ca^{2+} and Mn^{2+}, as well as Mg^{2+}, can stabilize a specific RNA structure in a group I intron (48). The order by which the divalent cations stabilize the tertiary structure of the *td* intron is in full accordance with the order of preference for the structural sites defined in previous works (46–48). However, Celander and Cech observed that the tertiary structure of the *Tetrahymena* intron, when stabilized by Ca^{2+}, is not quite as compact as the one stabilized by Mg^{2+} (2).

The studies presented here demonstrate that the introduction of base changes within helical stem regions may have profound effects on the structure and stability of transcripts of the *td* group I intron, especially when these substitutions affect the central pseudoknot, whose P7 helix appears to be crucial for stability. Derivation of the thermodynamic parameters associated with tertiary folding demonstrates that this process is enthalpically stabilized and has an unfavorable entropic term. The selectivity for Mg^{2+} indicates that there is a site-specific component in the further stabilization of tertiary structure by Mg^{2+}.

ACKNOWLEDGEMENTS

P.B. is grateful to Philippe Benas for his precious help in the deconvolution of the melting profiles. P.B. was supported by a fellowship from the Ministère de l'Education Nationale, de l'Enseignement Supérieur et de la Recherche. Part of this work was carried out by P.B. during a stay at the Vienna Biocenter (Institut für Mikrobiologie und Genetik, Universität Wien) in the laboratory of R.S. with support from the Bundesministerium für Wissenschaft Forschung und Kunst (Vertrag GZ200.016/1-IV/6/96).

REFERENCES

1. Latham,J.A. and Cech,T.R. (1989) *Science*, **245**, 276–282.
2. Celander,D.W. and Cech,T.R. (1991) *Science*, **251**, 401–407.
3. Heuer,T.S., Chandry,P.S., Belfort,M., Celander,D.W. and Cech,T.R. (1991) *Proc. Natl Acad. Sci. USA*, **88**, 11105–11109.
4. Michel,F. and Westhof,E. (1990) *J. Mol. Biol.*, **216**, 585–610.
5. Doudna,J.A. and Cech,T.R. (1995) *RNA*, **1**, 36–45.
6. Doherty,E.A. and Doudna,J.A. (1997) *Biochemistry*, **36**, 3159–3169.
7. Golden,B.L., Gooding,A.R., Podell,E.R. and Cech,T.R. (1998) *Science*, **282**, 259–264.
8. Serra,M.J. and Turner,D.H. (1995) *Methods Enzymol.*, **259**, 242–261.
9. Westhof,E. and Michel,F. (1994) In Nagai,K. and Mattaj,I.W. (eds), *RNA–Protein Interactions*, IRL Press, Oxford, pp. 25–51.
10. Cole,P.E., Yang,S.K. and Crothers,D.M. (1972) *Biochemistry*, **11**, 4358–4368.
11. Stein,A. and Crothers,D.M. (1976) *Biochemistry*, **15**, 160–167.
12. Laing,L.G. and Draper,D.E. (1994) *J. Mol. Biol.*, **237**, 560–576.
13. Lu,M. and Draper,D.E. (1994) *J. Mol. Biol.*, **244**, 572–585.
14. Banerjee,A.R., Jaeger,J.A. and Turner,D.H. (1993) *Biochemistry*, **32**, 153–163.
15. Jaeger,L., Michel,F. and Westhof,E. (1993) *J. Mol. Biol.*, **234**, 331–346.
16. Tanner,M. and Cech,T.R. (1996) *RNA*, **2**, 74–83.
17. Costa,M., Fontaine,J.-M., Loiseaux-deGoër,S. and Michel,F. (1997) *J. Mol. Biol.*, **274**, 353–364.
18. Costa,M., Christian,E.L. and Michel,F. (1998) *RNA*, **4**, 1055–1068.
19. Draper,D.E. (1996) *Nat. Struct. Biol.*, **3**, 397–400.
20. Brion,P. and Westhof,E. (1997) *Annu. Rev. Biophys. Biomol. Struct.*, **26**, 113–137.
21. Zarrinkar,P.P. and Williamson,J.R. (1994) *Science*, **265**, 918–924.
22. Jaeger,L., Michel,F. and Westhof,E. (1994) *J. Mol. Biol.*, **236**, 1271–1276.
23. Costa,M. and Michel,F. (1995) *EMBO J.*, **14**, 1276–1285.
24. Sambrook,J., Fritsch,E.F. and Maniatis,T. (1989) *Molecular Cloning: A Laboratory Manual*. Cold Spring Harbor University Press, Cold Spring Harbor, NY.
25. Marky,L.A. and Breslauer,K.J. (1987) *Biopolymers*, **26**, 1601–1620.
26. Giese,M.R., Betschart,K., Dale,T., Riley,C.K., Rowan,C., Sprouse,K.J. and Serra,M.J. (1998) *Biochemistry*, **29**, 5605–5613.
27. Xia,T., McDowell,J.A. and Turner,D.H. (1997) *Biochemistry*, **36**, 12486–12497.
28. Rosenbaum,V. and Riesner,D. (1987) *Biophys. Chem.*, **26**, 235–246.
29. Sammons,D.W., Adams,L.D. and Nishizawa,E.E. (1981) *Electrophoresis*, **2**, 135–141.
30. Riesner,D., Steger,G., Zimmat,R., Owens,R.A., Wagenhöfer,M., Hillen,W., Vollbach,S. and Henco,K. (1989) *Electrophoresis*, **10**, 377–389.
31. Michel,F., Jaeger,L., Westhof,E., Kuras,R., Tihy,F., Xu,M.-Q. and Shub,D.A. (1992) *Genes Dev.*, **6**, 1373–1385.
32. Emerick,V.L. and Woodson,S.A. (1993) *Biochemistry*, **32**, 14062–14067.
33. Jaeger,J.A., Zuker,M. and Turner,D.H. (1990) *Biochemistry*, **29**, 10147–10158.
34. Laing,L.G., Gluick,T.C. and Draper,D.E. (1994) *J. Mol. Biol.*, **237**, 577–587.
35. Rosenbaum,V., Klahn,T., Lundberg,U., Holmgren,E., von Gabain,A. and Riesner,D. (1993) *J. Mol. Biol.*, **229**, 656–670.
36. Felden,B., Himeno,H., McCuthcheon,J.P., Atkins,J.F. and Gesteland,R.F. (1997) *RNA*, **3**, 89–103.
37. Aphasizhev,R., Theobald-Dietrich,A., Kostyuk,D., Kochetkov,S.N., Kisselev,L., Giege,R. and Fasiolo,F. (1997) *RNA*, **3**, 893–904.
38. Szewczak,A.A., Podell,E.R., Bevilacqua,P. and Cech,T.R. (1998) *Biochemistry*, **37**, 11162–11170.
39. Jaeger,L., Michel,F. and Westhof,E. (1996) In Eckstein,F. and Lilley,D.M.J. (eds), *Nucleic Acids and Molecular Biology*. Springer-Verlag, Berlin Heidelberg, Vol. 10, pp. 33–51.
40. Legault,P., Herschlag,D., Celander,D.W. and Cech,T.R. (1992) *Nucleic Acids Res.*, **20**, 6613–6619.
41. Banerjee,A.R. and Turner,D.H. (1995) *Biochemistry*, **34**, 6504–6512.
42. Sclavi,B., Sullivan,M., Chance,M.R., Brenowitz,M. and Woodson,S.A. (1998) *Science*, **279**, 1940–1943.
43. Pan,J., Thirumalai,D. and Woodson,S.A. (1997) *J. Mol. Biol.*, **273**, 7–13.
44. Pan,J. and Woodson,S.A. (1998) *J. Mol. Biol.*, **280**, 597–609.
45. Pyle,A.M. (1993) *Science*, **261**, 709–714.
46. Grosshans,C.A. and Cech,T.R. (1989) *Biochemistry*, **28**, 6888–6894.
47. Guerrier-Takada,C., Haydock,K., Allen,L. and Altman,S. (1986) *Biochemistry*, **25**, 1509–1515.
48. Downs,W.D. and Cech,T.R. (1990) *Biochemistry*, **29**, 5605–5613.
49. Shub,D.A., Gott,J.M., Xu,M.-Q., Lang,B.F., Michel,F., Tomaschewski,J., Pedersen-Lane,J. and Belfort,M. (1988) *Proc. Natl Acad. Sci. USA*, **85**, 1151–1155.
50. Cech,T.R., Damberger,S.H. and Gutell,R. (1994) *Nat. Struct. Biol.*, **1**, 273–280.
51. Belfort,M., Chandry,P.S. and Pedersen-Lane,J. (1987) *Cold Spring Harbor Symp. Quant. Biol.*, **52**, 181–192.
52. Galloway-Salvo,J.L., Coetzee,T. and Belfort,M. (1990) *J. Mol. Biol.*, **211**, 537–549.
53. Leontis,N.B. and Westhof,E. (1998) *J. Mol. Biol.*, **283**, 571–583.